

## REMOTE SENSING OF SEASONAL LEAF AREA INDEX ACROSS THE OREGON TRANSECT<sup>1</sup>

MICHAEL SPANNER AND LEE JOHNSON

*Johnson Controls World Services, Inc., NASA-Ames Research Center, Moffett Field, California 94035 USA*

JOHN MILLER

*Department of Physics and Astronomy, York University, North York, Ontario, Canada M3J 1P3*

RICHARD MCCREIGHT

*Department of Forest Science, Oregon State University, Corvallis, Oregon 97331 USA*

JIM FREEMANTLE

*Institute for Space and Terrestrial Science, North York, Ontario, Canada M3J 3K1*

JOHN RUNYON

*Department of Forest Science, Oregon State University, Corvallis, Oregon 97331 USA*

PENG GONG<sup>2</sup>

*Institute for Space and Terrestrial Science, North York, Ontario, Canada M3J 3K1*

*Abstract.* Remotely sensed data acquired from four remote-sensing instruments on three different aircraft platforms over a transect of coniferous forest stands in Oregon were analyzed with respect to seasonal leaf area index (LAI). Data from the four instruments were corrected for the varying seasonal and geographic atmospheric conditions present along the transect. Strong logarithmic relationships were observed between seasonal maximum and minimum LAI and the simple ratio (SR) (near infrared/red reflectance) calculated from the broad-spectral-band Thematic Mapper Simulator (TMS), as well as from the narrow-spectral-band Airborne Visible/Infrared Imaging Spectrometer (AVIRIS), the Compact Airborne Spectrographic Imager (CASI), and a Spectron SE590 spectro-radiometer ( $R^2 = 0.82-0.97$ ). The TMS SR reached an asymptote at an LAI of  $\approx 7-8$ . However, the SE590 and the CASI SR continued to increase up to the maximum LAI of 10.6. The variability of the relationship between the AVIRIS SR and LAI increased at stands with LAIs  $>7$ , making a trend in the AVIRIS SR-LAI relationship at LAIs  $>7$  difficult to discern. The SRs of the coniferous forest stands measured by the narrow-spectral-band instruments were higher than they were from the broad-spectral-band TMS. This is attributed partially to the integration of the TMS over a broad wavelength region in the red and more strongly to calibration differences between the sensors. Seasonal TMS SR trends for four time periods for some of the stands deviated from the expected seasonal LAI trends, possibly because of smoke and very low sun angles during some of the acquisition periods. However, the expected SR differences for the seasonal minimum and maximum LAI were observed for all of the sensors for nearly all of the forest stands. This study demonstrates that remotely sensed data from both broad- and narrow-spectral-band instruments can provide estimates of LAI for use in forest ecosystem simulation models to estimate evapotranspiration, photosynthesis, canopy turnover, and net primary production over large areas.

*Key words:* atmospheric correction; AVIRIS; CASI; coniferous forest; Oregon transect; OTTER project; remote sensing; SE590; seasonal leaf area index; Thematic Mapper Simulator (TMS).

### INTRODUCTION

A critical variable for assessing the functional characteristics of ecosystems is leaf area index (LAI), the projected leaf area per unit ground area (Running 1994 [this issue]). Knowledge of LAI is important for quantifying energy and mass exchange rates of water and carbon between the vegetative canopy and atmospheric interface, including fluxes of carbon, solar energy, and

water. Photosynthesis, transpiration, respiration, and light interception are all related to LAI. In the coniferous forests of the Pacific Northwest, for example, canopy carbon dioxide and water vapor exchange are proportional to increasing LAI up to  $\approx 6$  (Running et al. 1986). LAI increases as conditions favor net primary production (Turner and Long 1975, Gholz 1982). In Douglas-fir stands, LAI increases for  $\approx 40$  yr and

<sup>1</sup> Manuscript received 14 October 1992; revised and accepted 25 August 1993.

<sup>2</sup> Present address: Department of Geomatics Engineering, University of Calgary, Calgary, Alberta, Canada T2N 1N4.



then approaches an equilibrium value (Grier and Running 1977). When the coniferous forest stands reach an old-growth stage, LAI decreases (Ryan and Waring 1992).

The variety of methods for measuring LAI in forest stands require intensive field sampling (Marshall and Waring 1986). While stand estimates of LAI offer important insights into ecosystem processes, there is a need to characterize LAI over larger areas periodically. Regional air pollution, land use changes, and projected climate change affect vegetation processes over much larger areas than can be monitored from ground surveys. Seasonal measurements of LAI are desirable to gauge ecosystem processes such as canopy turnover and the interception of light and water. Remotely sensed observations offer a way to monitor LAI over large areas on a seasonal basis.

The objective of this study was to evaluate how well remotely sensed data acquired from four remote-sensing instruments mounted on several different aircraft were related to the LAI of a range of forest communities across Oregon. The stands selected for study displayed an extreme range in projected LAI from  $<1$  to  $>10$  (Runyon et al. 1994 [this issue]). The LAI of coniferous forest canopies varies seasonally due to the loss of needles during the fall and winter months and the addition of new growth during the spring (Sudworth 1967, Waring and Franklin 1979). The turnover of needles can be as much as 40% for some conifer species (particularly pine species) (Gholz et al. 1991), but generally is  $<30\%$  for conifers native to Oregon (Gholz et al. 1979). Understory vegetation also has a seasonal variation, with new growth occurring during the spring, followed by senescence during the midsummer and fall.

Remotely sensed data acquired from a Daedalus Thematic Mapper Simulator (TMS) flown on a NASA (National Aeronautics and Space Administration) ER-2 aircraft during the four time periods of the Multi-sensor Aircraft Campaign (MAC) supporting the Oregon Transect Ecosystem Research (OTTER) project (Peterson and Waring 1994 [this issue]) were analyzed with respect to seasonal variations in canopy spectral reflectance associated with changes in leaf area index. In addition, the OTTER experiment provided the opportunity to analyze data from three high-spectral-resolution instruments including the Airborne Visible/Infrared Imaging Spectrometer (AVIRIS) flown on a NASA ER-2 aircraft, the Compact Airborne Spectrographic Imager (CASI) flown on a single-engine aircraft, and a Spectron SE590 spectro-radiometer flown on an ultra-light aircraft. Remotely sensed relationships with seasonal maximum and minimum LAI from the high-spectral-resolution instruments and from the broad-spectral-band TMS were analyzed. The OTTER project provided a unique opportunity to analyze how well data from a number of remote-sensing instruments were related to the LAI of coniferous forests that

are representative of a broad range of mid-latitude coniferous forest ecosystems.

#### BACKGROUND

Previous studies have demonstrated that broad-spectral-band remotely sensed data were related to the leaf area index of coniferous forests during the mid-summer (Peterson et al. 1987, Herwitz et al. 1989, Spanner et al. 1990a). These studies investigated relationships between leaf area index and the simple ratio (SR) of near-infrared (NIR) (760–900 nm) and red (630–690 nm) radiance from the Daedalus Thematic Mapper Simulator and the Thematic Mapper (TM) on the Landsat-5 satellite. The form of the relationship between the SR and LAI was dominated by chlorophyll absorption in the red in the denominator of the equation, combined with a flat response in the NIR due to near asymptotic reflectances from multiple scattering caused by the conifer needles in the numerator, producing a positive relationship between the simple ratio and LAI. The asymptote of the indices at an LAI of  $\approx 7$ –8 resulted from insensitivity of the remotely sensed data to additional foliage. Understory vegetation and background reflectance caused variations in the SRs which reduced the strength of the relationship with the TM data in stands with  $<90\%$  overstory canopy cover.

Recently, analyses have been reported relating seasonal relationships between LAI and remotely sensed data from the Advanced Very High Resolution Radiometer (AVHRR) (Spanner et al. 1990b) and Thematic Mapper data (Curran and Dungan 1992). In the first study, strong relationships were observed between AVHRR normalized-difference vegetation index  $\{NDVI = [(NIR - red)/(NIR + red)]\}$  and LAI for the summer months. However, atmospheric effects resulting from large variations in the solar zenith angle affected the seasonal pattern of AVHRR NDVI. AVHRR NDVI values during the winter months were reduced to values below what could be explained by a reduction in leaf area index. In the Curran and Dungan (1992) study, Thematic Mapper NDVI corrected for solar zenith angle effects was found to be sensitive to seasonal changes in slash pine stands with low leaf area index.

The use of narrow-band sensors or imaging spectrometers to derive vegetation indices is of increasing interest as such sensors become available. To date, such sensors have received little attention in the literature with respect to estimation of LAI. One of the primary advantages of narrow-band sensors is the ability to select spectral bands that are completely uncontaminated by significant atmospheric absorption features. Further, the use of narrower spectral bands should result in less error in deducing the mean reflectance in any spectral band when the variation of the radiation is nonlinear with wavelength in a particular band. It might therefore be expected that the spectral indices from narrow-band sensors could lead to improvements in the relationships between spectral indices and LAI.

However, since all narrow-band sensors are currently under development and refinement and are carried on airborne platforms, the expected advantages are yet to be realized or evaluated.

In one study using the CASI sensor, Gong et al. (1992) investigated the correlations between variations in reflectance spectra and spectral derivatives with LAI where changes are primarily due to changes in canopy closure within one of the OTTER sites (site 5: Metolius). This study showed that the use of spectral derivatives led to increased LAI estimation accuracies for this open-canopy stand. Gamon et al. (1993) used a field spectro-radiometer to develop relationships of both broad-band and narrow-spectral-band NDVI with various measures of grassland canopy structure. Narrow-band NDVI was calculated with 12-nm bandwidth channels centered at 677 and 833 nm. Broad-band NDVI was calculated from simulated red and NIR AVHRR channels, which were derived by integrating over the appropriate narrow-band SE590 channels. It was found that the correlations of both broad- and narrow-spectral-band NDVI with green LAI, total biomass, and total LAI were essentially identical.

Remote-sensing instruments not only measure the reflectance of vegetation, but they also measure the scattering and absorption of energy by the Earth's atmosphere (Diner and Martonchik 1984, Tanre et al. 1990). In the shorter wavelength region (i.e., blue (450–520 nm)) the atmosphere may contribute >75% of the remotely sensed signal. In the visible region, light is scattered by gas molecules in the atmosphere, most notably oxygen and nitrogen, termed "Rayleigh scattering" (Frohlich and Shaw 1980). Aerosols (dust, haze, and smoke) also absorb and scatter solar radiation. A calibrated sunphotometer measures the attenuation of solar radiation by the atmosphere (Russell et al. 1986). From sunphotometer measurements, coupled with a radiative transfer model, the effect of the atmosphere can be removed from remotely sensed data (Green 1990, Wrigley et al. 1992).

#### METHODS

The six study areas selected for the OTTER study are arrayed across Oregon along an east–west transect at  $\approx 45^\circ$  N (Peterson and Waring 1994 [this issue]). The forest stands represent a variety of canopy leaf area indices (LAIs) ranging from >10 on the west side of the Cascade Mountains (site 3-F) to <1 on the open Juniper woodland site (site 6). As a result of the variations in the regional climate, the forest stands on the west side of the Cascade Mountains (sites 1–3) display high LAIs with <5% light penetration to the ground. In contrast, the forest stands on the east side of the transect have low LAIs, with open areas of soil and litter and understory vegetation (sites 5-F and 6). Study area 1 is near the coast and consists of one red alder (*Alnus rubra*) stand (1-A), an old-growth stand consisting of western hemlock (*Tsuga heterophylla*), Doug-

las-fir (*Pseudotsuga menziesii*), and Sitka spruce (*Picea sitchensis*) (1-O), and a medium aged stand composed of sitka spruce and western hemlock (1-G). Site 2 consists mostly of Douglas-fir, with some big-leaf maple (*Acer macrophyllum*) and Oregon white oak (*Quercus garryana*). Study area 3 includes a fertilized (3-F) and a control stand of dense 30-yr-old Douglas-fir. Site 4 is composed of mostly mountain hemlock (*Tsuga mertensiana*). Study area 5 includes open-canopied fertilized (5-F) and control stands of ponderosa pine (*Pinus ponderosa*); site 6 is an open stand of western juniper (*Juniperus occidentalis*).

#### Field measurements

Intercepted Photosynthetically Active Radiation (IPAR) measurements were made near noon at all of the OTTER sites during July–August 1991 (Runyon et al. 1994 [this issue]). These measurements were made with a ceptometer measuring instantaneous fluxes of solar radiation in the photosynthetically active region of 400–700 nm. Canopy transmittance was calculated by dividing the average below-canopy measurements by the average incident PAR. Leaf area index (LAI) was calculated for each site from the canopy transmittance measurements using the Beer–Lambert law, which assumes a negative exponential relationship between transmitted light and LAI:

$$\text{LAI} = -\ln(Q_i/Q_0)/k, \quad (1)$$

where  $Q_0$  is the average incident PAR,  $Q_i$  is the average below-canopy PAR, and  $k$  is a light extinction coefficient.  $k$  values range from 0.40 to 0.65 depending on species (Jarvis and Leverenz 1983). An average  $k$  value of 0.5 was used for all stands.

Minimum LAI was not directly measured. The percentage change in LAI was estimated from new foliage growth. Assuming that the canopies were at steady state, foliage loss should equal annual foliage production. Minimum LAI values occur in the winter after fall senescence of the foliage (Gholz et al. 1991). In order to gauge the pattern of foliage production across the transect, we measured the fraction of new growth in the summer during maximum canopy development (Runyon et al. 1994 [this issue]). No measurements from site 4 were collected due to extensive spruce budworm defoliation. At this site, estimates of new foliage growth fraction for a similar subalpine stand were used to compute total foliage production (Gholz 1982). Winter minimum LAIs averaged 27% less than the summer maximum for the coniferous forest stands (Table 1).

#### Remotely sensed measurements

Remotely sensed data to support the objectives of the OTTER project were acquired as part of a NASA-sponsored Multi-sensor Aircraft Campaign (MAC; Peterson and Waring 1994 [this issue]). Aircraft data were acquired during four time periods in 1990 and one in

TABLE 1. Seasonal maximum and minimum leaf area index (LAI) values for each site along the Oregon transect (Runyon et al. 1994 [this issue]).

Site	Site name (description)	Maximum LAI		Minimum LAI	Change in LAI	% change in LAI
		Mean	SD			
1-O	Cascade Head (Old-growth forest)	6.6	0.3	4.8	1.8	27.2
1-G	Cascade Head (Medium growth)	7.3	0.3	5.3	2.0	27.4
1-A	Cascade Head (Alder stand)	4.6	0.2	0	4.6	100.0
2	Waring's Woods (Douglas-fir-Oak-Maple)	5.7	0.4	4.0	1.7	29.8
3-C	Scio (Douglas-fir)	10.6	0.4	7.4	3.2	30.1
4	Santiam Pass (Subalpine forest)	1.9	0.1	1.5	0.4	21.1
5-F	Metolius (Young ponderosa pine)	0.7	0.1	0.5	0.2	28.6
6	Juniper (Juniper woodland)	0.5	0.1	0.4	0.1	20.0

1991. Data were collected in March during pre-bud conditions, in June when understory development peaked, in August at maximum leaf area index, and in October under conditions of senescent understory vegetation. Additional flights were undertaken in May 1991 to acquire remotely sensed data that were not obtained in 1990.

The wavelength regions analyzed for all of the remote-sensing instruments were centered near 680 nm in the red and 790 nm in the near-infrared region (NIR), respectively (Table 2). These wavelengths are well situated to measure the reflectance minima due to chlorophyll absorption in the red, to measure the vegetation reflectance plateau in the NIR, and to avoid atmospheric water absorption in the NIR. For AVIRIS, CASI, and the SE590 (high-spectral-resolution instruments, see *Introduction*, above), wavelengths as close as possible to 680 and 790 nm were analyzed. For the broad-spectral-band Thematic Mapper Simulator (TMS), the wavelengths used were channels in the 630–690 nm and 760–900 nm region. The TMS, AVIRIS, and CASI data were atmospherically corrected using identical procedures, utilizing calibrated at-sensor radiances with a radiative transfer model and optical measurements of the atmosphere. The SE590 data were atmospherically corrected using a different methodology relating reflectance at varying altitudes to surface reflectance because SE590 data are used to measure reflectance factors, not absolute radiance.

#### *Sunphotometer*

Sunphotometer measurements of atmospheric optical properties were made at most of the sites within 1–2 h of all aircraft overflights. Two identical sunphotometers were utilized during the OTTER project. The sunphotometers were 10-channel instruments with narrow filters in the visible through near-infrared

wavelengths. At each site, measurements were made with the sunphotometer every 3–4 min for  $\approx 30$  min. Processing of these data allowed calculation of total atmospheric optical depth. Optical depth is a measure of the attenuation of solar radiation by the atmosphere. The Rayleigh optical depth was calculated using the measured pressure; the optical depth of ozone and nitrogen dioxide were calculated using climate tables developed by Noxon (1979) and Van Heuklon (1979), respectively. The Rayleigh, ozone, and nitrogen dioxide optical depths were then subtracted from the total optical depth to yield the aerosol optical depth. The sunphotometer measurements of optical depth were used to atmospherically correct the TMS, AVIRIS, and CASI imagery.

#### *Thematic Mapper Simulator*

The Daedalus Thematic Mapper Simulator (TMS) was flown on a NASA ER-2 aircraft at an altitude of  $\approx 20$  km mean sea level (MSL) on 21 March, 25 and 26 June, 13 and 14 August, and 19 and 24 October 1990, and 22 May 1991. The TMS data were acquired to analyze seasonal variations in LAI along the Oregon transect. The TMS is a 12-channel multispectral scanner, with 8-bit radiometry, and a spatial resolution of  $\approx 25$  m at nadir (Table 2). The TMS flights occurred between 1100 and 1400 local solar time. The TMS data for the Thematic Mapper equivalent channels were converted to radiance in watts per square metre per steradian per micrometre based on calibrations performed by the High Altitude Missions Branch at NASA-Ames Research Center (Moffett Field, California, USA). The TMS instrument was calibrated shortly before or after each set of flights using an integrating sphere certified against National Bureau of Standards (NBS) standards.

From the calibrated TMS at-sensor radiance data,

TABLE 2. Characteristics of the remote-sensing instruments used in this study. The spectral regions shown (red and near infrared) indicate the full width half maximum (FWHM).

Sensor*	Altitude	Spectral bands	Spatial resolution
TMS	20 km	Red 630–690 nm NIR 760–900 nm	24 m
AVIRIS	20 km	Red 670–680 nm August NIR 781–790 nm August Red 670–680 nm March NIR 784–796 nm March	20 m
CASI	1.4–1.8 km	Red 676–682 nm NIR 784–790 nm	2–3 m
SE590	100 m	Red 673–685 nm NIR 781–793 nm	1.5–17.5 m

\* TMS = Thematic Mapper Simulator; AVIRIS = Airborne Visible/Infrared Imaging Spectrometer; CASI = Compact Airborne Spectrographic Imager; SE590 = Spectron SE590 spectro-radiometer.

the locations of the OTTER sites were carefully delineated on an interactive display using large-scale aerial photographs and field inspection. The size of the sites on the TMS imagery ranged from  $15 \times 15$  pixels ( $375 \times 375$  m) for the larger sites in the east (sites 5 and 6) to  $3 \times 3$  pixels ( $75 \times 75$  m) for the smaller sites (sites 1–4). Consistency in the location of the site for the four seasonal acquisitions was ensured by delineating the same number of pixels from each site for each season and by careful inspection of the sites on the interactive display. The mean and standard deviation of the radiance from the NIR TMS channel 7 (760–900 nm) and the red TMS channel 5 (630–690 nm) were calculated for each of the OTTER sites for each of the time periods.

The mean at-sensor radiances were corrected for atmospheric effects using LOWTRAN-7 (Kneizys et al. 1989), based on sunphotometer measurements of aerosol optical depth at each site at or near the time of overflight (Johnson et al. 1993). The optical depths were used to estimate horizontal visibility by fitting to LOWTRAN-7 calculated transmittance. Surface canopy reflectance ( $p$ ) was retrieved from at-sensor radiance  $L_s$  by:

$$p = (L_r/L_{ra})\alpha, \quad (2)$$

where ( $L_r = L_s - L_p$ ) is the net canopy-reflected radiance,  $L_{ra}$  is the net modelled radiance reflected from a surface with albedo  $\alpha$ , for the given solar zenith and surface elevation, and  $L_p$  is the atmospherically scattered radiance reaching the sensor. The ratio of the TMS NIR (760–900 nm) and red (630–690 nm) reflectances were calculated from the mean atmospherically corrected surface reflectance for each site during each time period.

#### High-spectral-resolution instruments

The Airborne Visible/Infrared Imaging Spectrometer on NASA ER-2 aircraft collected data over the Oregon transect on 21 March and 13 and 14 August 1990. AVIRIS data were acquired during the OTTER experiment to determine their capability to estimate

canopy biochemical properties of coniferous forests (Johnson et al. 1993). The OTTER experiment also provided an opportunity to determine the sensitivity of AVIRIS data to LAI. AVIRIS is a 224-channel instrument that obtains data throughout the 400–2450 nm region with a bandwidth of  $\approx 10$  nm and a spatial resolution of  $\approx 20$  m (Vane 1987). Data pre-processing, including calibration according to the methods described by Chrien et al. (1990), was performed at the Jet Propulsion Laboratory (Pasadena, California, USA).

Data from AVIRIS channels 29 (red region) and 44 (NIR region) for the August acquisition, and channels 29 and 45 for the March acquisition were extracted for analysis. The nominal centers for these channels are 675 nm and 786 nm for August and 675 nm and 790 nm for March, respectively (Table 2). A total of 11 observations were compiled: 4 in March and 7 in August. Nine pixels representing a  $3 \times 3$  pixel matrix centered on each site were averaged to provide a mean digital count per channel, per observation. The published gain value was used to convert the digital counts into units of at-sensor radiance calculated by the Jet Propulsion Laboratory (Pasadena, California, USA). The at-sensor radiance was corrected for atmospheric effects using Lowtran-7 (Kneizys et al. 1989), based on sunphotometer measurements of aerosol optical depth using the same procedure that was used to atmospherically correct the TMS data. The simple ratio (SR) of the NIR and red atmospherically corrected surface reflectances was calculated for each of the 11 AVIRIS March and August observations.

The Compact Airborne Spectrographic Imager (CASI) was flown on a single-engine aircraft over the Oregon transect during mid-August 1990 and late May 1991. CASI data were acquired during OTTER to estimate chlorophyll content of the coniferous forest canopy using red-edge techniques (Matson et al. 1994). The acquisition of CASI data during the OTTER experiment provided an opportunity to determine the sensitivity of CASI data to LAI. CASI operated in both spatial and spectral modes on successive overpasses. In the spectral mode, CASI has a spectral range of 425–

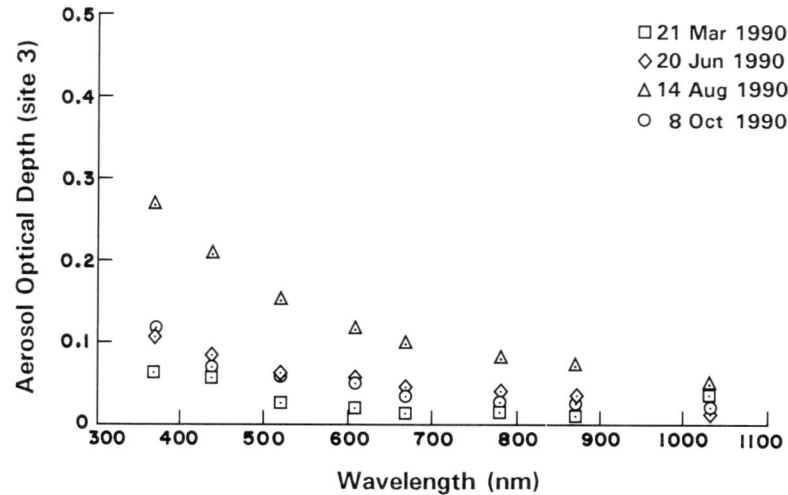


FIG. 1. Aerosol optical depth at site 3 during the four time periods of the OTTER (Oregon Transect Ecosystem Research) experiment.

925 nm at 3–6 nm resolution. Spectral-mode data were analyzed for this study. The single-engine aircraft with CASI flew at altitudes from 1.4 to 1.8 km above ground level (AGL), yielding pixel dimensions for the spatial mode of  $\approx 2$  m in the across-track direction by 3 m in the along-track dimension. Calibrated CASI data were atmospherically corrected using the same procedure that was used to atmospherically correct the TMS and AVIRIS data. Site-average CASI reflectance from channels centered at 679 and 787 nm (6 nm full-width half-maximum (FWHM)) were used to calculate the SR for the OTTER sites. CASI site averages were obtained in a manner similar to the TMS analyses.

The Spectron SE590 spectrometer was flown on the ultra-light aircraft in 1990 and 1991 during the OTTER MAC at nearly the same time that the other aircraft flew. SE590 data were acquired from the ultra-light aircraft during OTTER to provide a flexible and inexpensive platform to analyze leaf area index and other canopy properties. The SE590 collects data in 256 channels between 375 and 1100 nm with 12-nm resolution and a 3-nm sampling interval. SE590 spectrometer measurements were made at 100 m AGL at a speed of  $\approx 50$  km/h. The pixel size at nadir was 1.5 m across track using a sensor field-of-view of  $1^\circ$ . Pixel size in the along-track direction varied from 1.5 to 17.5 m depending on the sensor integration times of 0.1 to 1.0 s in response to variable surface albedo. Generally, 20–70 measurements were used to characterize the surface reflectance of each site. Open forests required greater sampling to reduce the standard error of the mean.

The vertical distribution of aerosols in the lower atmosphere over a site was documented by reflectance measurements off a halon reference panel at vertical intervals of 300 m altitude. The panel was positioned 15 cm below the spectro-radiometer during in-flight

calibration. Site reflectance was calculated from SE590 coverage, after correcting for atmospheric effects and verifying site coverage using the video flight record. Spectron SE590 channels centered at 787 and 679 nm were selected to calculate the simple ratio for sites 2–6.

## RESULTS AND DISCUSSION

### *Atmospheric measurements*

Fig. 1, which shows the aerosol optical depth measured at site 3, is representative of the variability of the aerosol optical depth measured during the four time periods of the OTTER Multi-sensor Aircraft Campaign (MAC) in 1990. The aerosol optical depth at 679 nm ranged from  $\approx 0.02$  to 0.04 for the March, June, and October time periods. For the August time period, the optical depth at 679 nm was  $\approx 0.10$ , an increase of  $>250\%$  over the other time periods. Aerosol optical depth values of 0.02 to 0.04 at 679 nm are very low and are indicative of clear atmospheric conditions, with few particulates or aerosols. Aerosol optical-depth values of 0.10 at 679 nm are relatively high and cause a larger atmospheric effect on remotely sensed data. The high aerosol optical-depth values during August were caused by smoke from grass sod seed burning in the Willamette Valley and a forest fire south of site 5. The smoke was present at all of the sites during August except for site 1 on the coast.

### *SR-LAI relationships*

A summary of the SR (simple ratio)–LAI (leaf area index) relationships for the four instruments is presented in Table 3. For all of the instruments the August SR was selected to represent the summer maximum LAI and the March SR was selected to represent the seasonal minimum LAI, except for CASI (Compact Airborne Spectrographic Imager) data where the May

TABLE 3. Relationship between spectral indices from the remote-sensing instruments ( $y$ ) and seasonal leaf area index (LAI) ( $x$ ).

Sensor*	Regression	SR†- LAI $R^2$	SE of $y$ esti- mate
TMS	$y = 3.1196 + 4.5857 \log x$	0.97	0.47
AVIRIS	$y = 4.2514 + 9.9020 \log x$	0.82	2.47
CASI	$y = 4.8985 + 12.004 \log x$	0.92	2.154
SE590	$y = 3.7177 + 11.344 \log x$	0.95	1.37

\* For explanation of acronym, see Table 2.

† SR = simple ratio (near-infrared radiance)/(red radiance).

SR was used to represent the seasonal minimum LAI because CASI data were not acquired in March. Fig. 2 shows the relationship between August maximum and March minimum Thematic Mapper Simulator (TMS) SR and seasonal LAI for the conifer stands. These data describe an asymptotic relationship, with saturation in the SR occurring at an LAI of  $\approx 7-8$ , consistent with theoretical and experimental data for other broad-spectral-band instruments (Tucker 1979, Hoffer 1978, Peterson et al. 1987). The strength of the logarithmic relationship ( $R^2 = 0.97$ ) indicates that the TMS data were sensitive to the seasonal variation of leaf area index up to an LAI of  $\approx 7-8$ .

Fig. 3 shows the logarithmic relationship between the AVIRIS (Airborne Visible/Infrared Imaging Spectrometer) SR and seasonal LAI of the conifer stands ( $R^2 = 0.82$ ). Fig. 3, like Fig. 2, does not display a trend of increasing SR above an LAI of  $\approx 7$ . The two data points with SRs above 16 prevent the development of such a relationship. Fig. 4 shows the logarithmic relationship between the CASI SR and the seasonal LAI of the conifer stands ( $R^2 = 0.92$ ). The relationship between SR and LAI increases to the highest OTTER

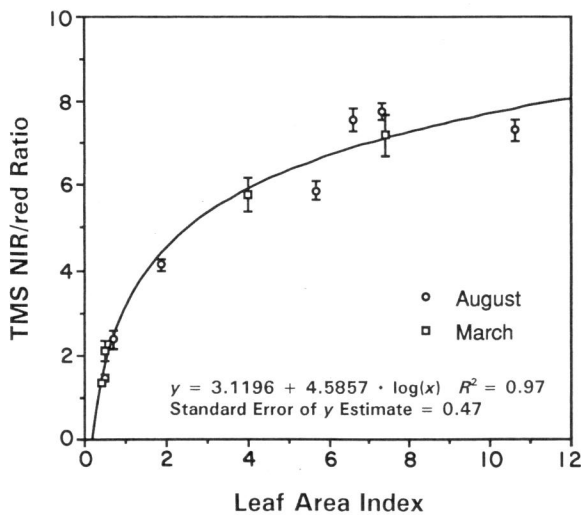


FIG. 2. Relationship between the Thematic Mapper Simulator (TMS) simple ratio (SR) (March and August) and seasonal leaf area index (LAI). (SR = near-infrared/red.)

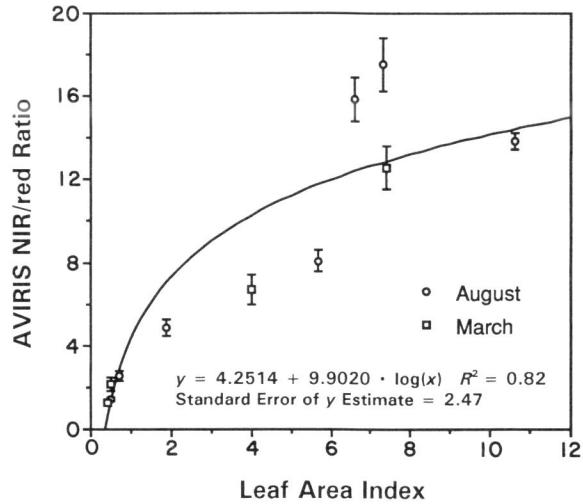


FIG. 3. Relationship between AVIRIS SR (March and August) and seasonal LAI.

LAI of 10.6, unlike the TMS and AVIRIS data. Fig. 5 shows the logarithmic relationship between the Spectron SE590 radiometer SR and seasonal LAI of the conifer stands ( $R^2 = 0.95$ ). As with CASI, the SE590 SR increases up to the maximum LAI of 10.6. Tables 4-7 show the red and NIR (near-infrared) reflectances, as well as the SRs for TMS, AVIRIS, CASI, and the SE590, respectively.

Fig. 6 shows the logarithmic relationship between the SR for all of the instruments and seasonal LAI. The broad-spectral-band TMS SR values are much lower than the SR values from the three narrow-spectral-band sensors. From examination of Tables 4-7, it can be seen that for all of the sensors the NIR reflectances are within  $\approx 10\%$  of each other. However, the TMS red reflectances are consistently larger than the

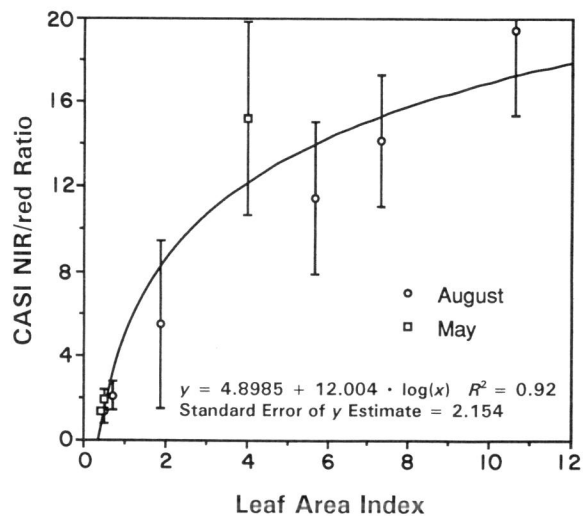


FIG. 4. Relationship between CASI SR (May and August) and seasonal LAI.

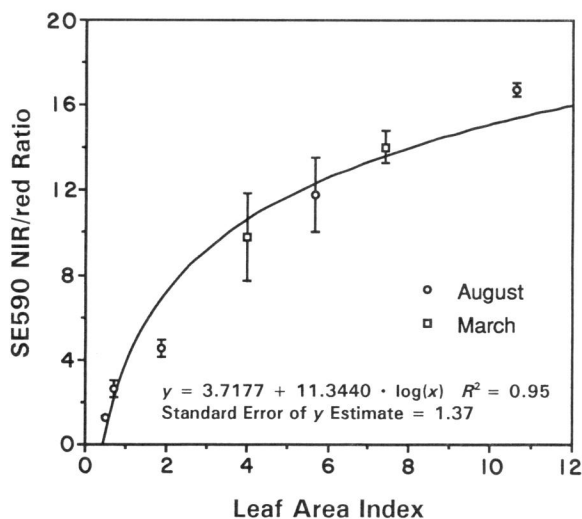


FIG. 5. Relationship between the SE590 SR (March and August) and seasonal LAI.

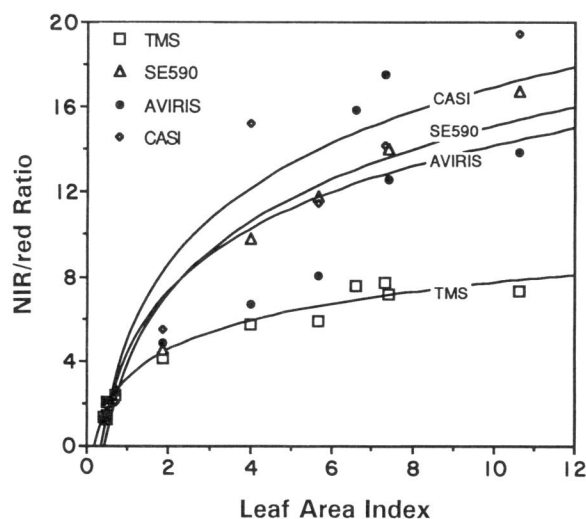


FIG. 6. Relationship between the SR for all sensors and seasonal LAI.

red reflectance from the other instruments by as much as 40%. The higher red reflectances of the TMS are partially explainable by the integration of TMS red reflectance over a broad wavelength region.

The red channels for AVIRIS, CASI, and the SE590 are centered at the chlorophyll absorption reflectance minima at 680 nm. The TMS red channel encompasses 630–690 nm, a region with decreased absorption at the

edges. Because of these differences, narrow band red reflectances from AVIRIS, CASI, and the SE590 would be expected to be lower than the broad-band TMS red reflectances. A simulation was performed in which AVIRIS data were convolved to the TMS red-channel filter function to derive an AVIRIS broad-spectral-band red reflectance to compare with the TMS measured red reflectance. For site 3-F in August the AVIRIS narrow-

TABLE 4. Atmospherically corrected Thematic Mapper Simulator (TMS) red and near-infrared (NIR) reflectance (as % of incoming solar radiation in that wavelength range) and the simple ratio (SR = NIR/red ratio) for the OTTER sites.

Site	Date	Red reflectance (%)		NIR reflectance (%)		SR	
		Mean	SD	Mean	SD	Mean	SD
1-O	June 1990	2.37	0.05	20.06	0.74	8.45	0.37
	August 1990	2.32	0.07	17.58	0.39	7.57	0.28
1-G	June 1990	2.54	0.05	21.06	0.70	8.27	0.31
	August 1990	2.54	0.05	19.79	0.38	7.58	0.28
1-A	June 1990	2.95	0.04	36.43	0.56	12.34	0.30
	August 1990	2.79	0.06	34.37	1.22	12.32	0.52
2	March 1990	2.32	0.06	13.38	0.79	5.77	0.41
	June 1990	2.81	0.04	22.00	0.06	7.81	0.24
	August 1990	3.07	0.06	18.05	0.59	5.87	0.22
	October 1990	2.27	0.10	16.45	1.64	7.23	0.79
3-F	March 1990	2.53	0.07	18.22	1.14	7.19	0.50
	June 1990	3.32	0.04	28.71	0.60	8.65	0.21
	August 1990	3.27	0.08	27.72	0.62	7.32	0.26
	October 1990	2.11	0.09	20.04	0.52	9.47	0.50
4	March 1990	10.39	1.44	14.00	1.50	1.34	0.24
	June 1990	3.59	0.09	12.74	0.54	3.55	0.18
	August 1990	2.85	0.06	11.74	0.30	4.13	0.14
	October 1990	1.80	0.04	7.47	0.52	4.15	0.31
5-F	March 1990	5.99	0.59	12.54	0.67	2.09	0.23
	June 1990	6.69	0.76	16.30	0.47	2.44	0.29
	August 1990	7.38	0.65	17.59	0.46	2.38	0.22
	October 1990	5.88	0.61	14.67	1.20	2.49	0.33
6	March 1990	8.77	0.36	11.92	0.48	1.36	0.08
	June 1990	9.48	0.38	14.67	0.50	1.55	0.08
	August 1990	11.74	0.41	17.27	0.58	1.47	0.07
	October 1990	9.61	0.41	14.64	0.62	1.52	0.09

TABLE 5. Atmospherically corrected AVIRIS red and near-infrared (NIR) reflectance (% of incident) and the simple ratio (SR) for the OTTER sites.

Site	Date	Red reflectance (%)		NIR reflectance (%)		SR	
		Mean	SD	Mean	SD	Mean	SD
1-O	August 1990	1.4	0.09	22.2	0.38	15.86	1.06
1-G	August 1990	1.3	0.07	22.8	1.07	17.54	1.25
2	March 1990	2.4	0.20	16.1	1.16	6.71	0.74
	August 1990	2.6	0.12	21.0	0.97	8.08	0.53
3-F	March 1990	1.7	0.10	21.4	1.28	12.59	1.06
	August 1990	2.0	0.05	27.7	0.36	13.85	0.39
4	August 1990	2.4	0.15	11.7	0.6	4.88	0.39
5-F	March 1990	6.3	0.73	13.7	1.02	2.17	0.30
	August 1990	6.5	0.56	16.5	0.64	2.54	0.24
6	March 1990	10.3	0.44	13.3	0.78	1.29	0.09
	August 1990	11.3	0.35	16.4	0.51	1.45	0.06

spectral-band red reflectance was 2.0%, the TMS red reflectance was 3.27%, and AVIRIS data convolved with the TMS filter function red reflectance was 2.13%. Approximately 10% of the difference between the AVIRIS and the TMS red reflectance at site 3-F can be explained by the integration of TMS over the broad red-wavelength region. The rest of the difference is likely due to instrument calibration differences. The difference between 2.0 and 3.27% reflectance is small in absolute terms. However, with red reflectance as low as 2.0%, any variation in red reflectance will cause a large change in the SR.

The TMS and AVIRIS SR leveled off at LAI values of  $\approx 7-8$ . The SR from the CASI and SE590, however, were sensitive to LAI up to the OTTER maximum of 10.6. The AVIRIS SR did not increase up to the maximum LAI because of the two very high SR values. Law and Waring (1994) found that the SR measured by an SE590 was linearly related to the LAI of stacked shrub branches of manzanita (*Arctostaphylos patula*) and bitterbrush (*Purshia tridentata*) which reached LAI levels  $>8$ . From this study, however, it is not possible to generalize that the SR from high-resolution instruments are sensitive to LAIs  $>7$ . The AVIRIS data refute that hypothesis. A possible explanation for the increased sensitivity of the CASI and the SE590 data to high LAIs is that the SE590 and CASI were flown at fairly low altitudes with less intervening atmosphere

between the ground and the sensor, whereas the AVIRIS and TMS were flown at 20 km, but we have no data to support that explanation.

The standard deviations of the SRs were higher for CASI and the SE590 data than they were for the TMS and AVIRIS data. This is a result of the finer spatial resolution of the CASI and SE590 ( $<5$  m). AVIRIS and TMS, with spatial resolutions  $>20$  m, integrate their measurements over larger areas, thus reducing the variability of the between-pixel reflectances.

#### Seasonality of the TMS SR

Fig. 7 shows the seasonal trends of the TMS SR for sites 4, 5-F, and 6 for four time periods. Some SR seasonality can be observed for sites 5-F and 6 between March and the rest of the seasons. The seasonal addition of overstory LAI was very low at both sites (Table 1). The understory vegetation consisted of fescue grass (*Festuca* sp.), rabbit brush (*Chrysothamnus* sp.), and sagebrush (*Artemisia* sp.)—species with low chlorophyll content in this xeric environment. It was anticipated, however, that as the overstory and understory initiated growth between March and June, and then senesced in August through October, some seasonal variation would be observed in the TMS SR. From analysis of digitized color infrared photographs with a spatial resolution of 1 m acquired from the NASA C-130 aircraft it was determined that under-

TABLE 6. Atmospherically corrected CASI red and NIR reflectance (% of incident) and the SR for the OTTER sites.

Site	Date	Red reflectance (%)		NIR reflectance (%)		SR	
		Mean	SD	Mean	SD	Mean	SD
1-G	August 1990	1.73	0.30	24.56	3.29	14.20	3.11
2	May 1991	0.89	0.20	13.57	2.72	15.25	4.59
	August 1990	1.56	0.34	17.87	3.95	11.46	3.56
3-F	August 1990	1.34	0.23	26.01	2.99	19.41	4.01
5-F	May 1991	7.74	1.68	15.00	1.43	1.94	0.46
	August 1990	12.05	3.37	25.15	3.67	2.09	0.66
6	May 1991	11.76	1.37	15.89	1.22	1.35	0.19
	August 1990	11.19	3.67	15.14	3.14	1.35	0.52

TABLE 7. Atmospherically corrected SE590 red and NIR reflectance (% of incident) and the SR for the OTTER sites.

Site	Date	Red reflectance (%)		NIR reflectance (%)		SR	
		Mean	SD	Mean	SD	Mean	SD
2	March 1991	1.37	0.33	13.47	5.76	9.81	2.06
	August 1990	2.34	1.15	27.62	3.88	11.78	1.74
3-F	March 1991	1.80	0.27	25.30	5.11	14.06	0.77
	August 1990	1.64	0.29	27.45	4.08	16.77	0.32
4	August 1990	1.67	0.86	7.65	0.98	4.57	0.40
5-F	August 1990	4.38	1.93	11.53	2.81	2.63	0.42
6	August 1990	8.20	1.16	10.58	1.34	1.29	0.03

story vegetation constituted  $\approx 16$  and 21% of the overall cover for sites 5-F and 6, respectively. The lack of greenness of the understory vegetation, combined with the low amount of understory and overstory vegetation, help explain why a pronounced seasonality was not observed in the TMS SR for sites 5-F and 6.

Site 4 had a very low SR during March, caused by snow on the ground at the time of data acquisition (Fig. 7). The site became snow-free in early June. The highest SR for site 4 was observed in August, corresponding to the maximum overstory LAI and understory green-up. The green-up is late in the year at site 4 because of its high elevation (1500 m). The understory at site 4 consisted of thick patches of huckleberry (*Vaccinium membranaceum*) and beargrass (*Xerophyllum tenax*). The understory was fully developed by August and was senescing during the October overflight. The trend of the SR corresponds somewhat with this phenology, but is generally more stable between August and October than expected.

Fig. 8 shows the seasonal TMS SR for sites 2 and 3-F. Interpretation of Fig. 3 with respect to the seasonality of the vegetation is problematic. Both sites 2 and 3-F have their lowest SR values in March and increase in June as expected. However, the SR at both sites decreased significantly in August and reached the

highest levels in October. The behavior of the SRs in August and October is not explainable in terms of vegetation seasonality. There was virtually no understory at site 3-F, and overstory LAI remained fairly stable between June and October.

During August, there was considerable smoke in the atmosphere from nearby fires. In particular, at site 3 the amount of smoke above the site varied considerably during the day. Sunphotometer measurements at site 3 were made  $\approx 1$  h and 20 min after the ER-2 TMS overflight. It is possible that the aerosol optical depths were higher at the time of the overpass than they were when they were measured with the sunphotometer. Because smoke both absorbs and scatters radiation (Fraser and Kaufman 1985), the atmospheric correction may not have compensated for the conditions present during the August fires.

The high SR values in October resulted in part from the very low surface-reflected energy levels present during the 24 October overflight. The solar-zenith angle during this overflight was  $59^\circ$ . At-sensor radiances measured in the red band were very low and after atmospheric correction they were even lower (Table 4). High LAI sites such as sites 3-F and 2 have low red reflectance due to chlorophyll absorption. Large solar-zenith angles cause an increase in shadowing over for-

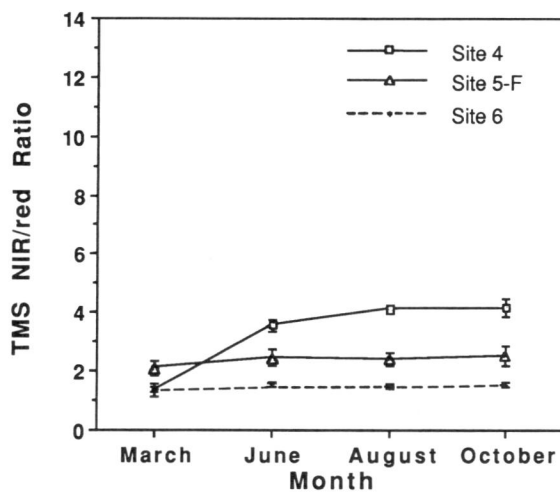


FIG. 7. Seasonal TMS SR for sites 4, 5-F, and 6.

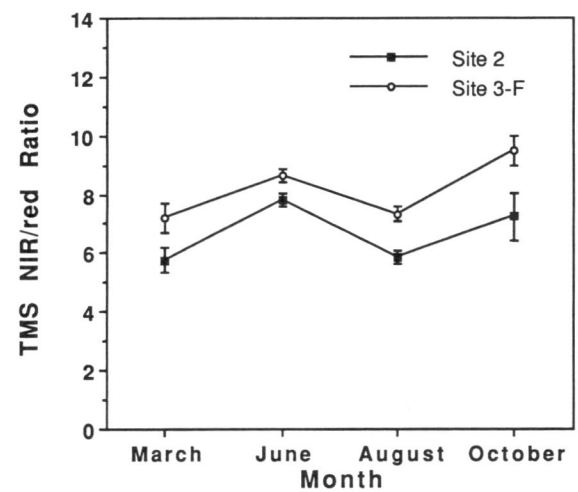


FIG. 8. Seasonal TMS SR for sites 2 and 3-F.

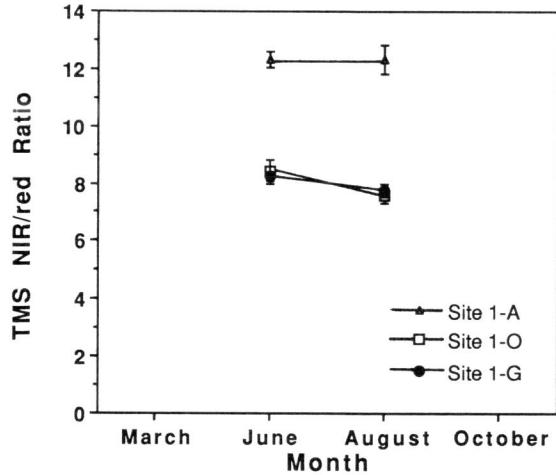


FIG. 9. Seasonal TMS SR for sites 1-A, 1-O, and 1-G.

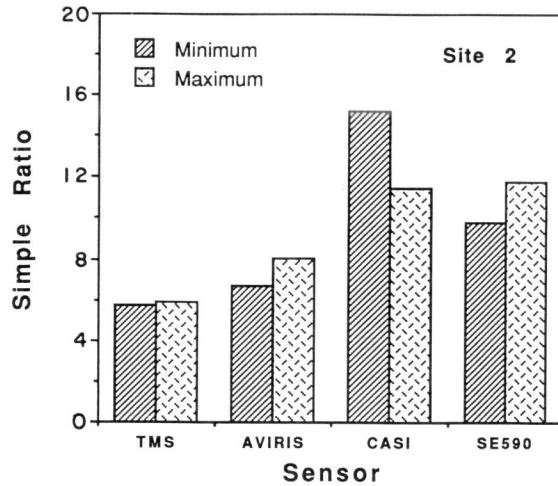


FIG. 10. Seasonal minimum and maximum simple ratio (SR = NIR/red reflectance) for sensors at site 2.

ested stands, reducing the red reflectance even more. Very low red reflectances in the denominator of the SR as observed at sites 3-F and 2 in October caused unexpectedly high SR values. In contrast, the solar-zenith angles for the March, June, and August overflights for sites 3-F and 2 were 45, 22, and 35°, respectively. Ranson et al. (1986) measured the reflectance of a simulated balsam fir (*Abies balsamea*) canopy with a broad-banded field radiometer and found that as the solar zenith angles increased, so did the normalized-difference vegetation index (NDVI) (hence, the SR). L. F. Johnson (*unpublished manuscript*), studying Advanced Solid-state Array Spectrometer (ASAS) data from the OTTER study area, found that as the amount of shadow increased, the SR increased. Limits to the accurate measurement, atmospheric correction, and analysis of the SR with respect to vegetation seasonality may have been exceeded in late October because of the large solar-zenith angles.

At study area 1 the TMS SRs in June and August for both the conifer and alder stands were fairly constant, with slightly lower SRs for sites 1-O and 1-G in August (Fig. 9). The SR reduction between June and August was much less than was observed at sites 2 and 3-F. This coastal site had very clear atmospheric conditions with no smoke. The atmospheric-correction algorithm may have been more effective under smokeless conditions. Both the conifer and the alder stand were at maximum LAI in June and August. The understory vegetation, consisting of sword fern (*Polystichum munitum*), huckleberry and Oregon oxalis (*Oxalis oregana*), remain green during June and August at this mesic site near the coast. TMS data for site 1 during March and October were not useable because of cloud cover.

The SR for the alder stand (site 1-A) was much higher than for the conifer stands (sites 1-O and 1-G) in both

June and August, with SR values of  $\approx 12$  for the alder stand and values of  $\approx 7-8$  for the conifer stands, respectively. The LAIs of the conifer stands were much higher than the deciduous alder stand, 6.6 and 7.3 vs. 4.6, respectively. The increased SR for the alder site resulted from elevated reflectance in the NIR. Broad-leaf trees have different reflective properties than needle-leaf conifers, caused by differences in leaf and canopy structure (Peterson et al. 1987). Relationships developed between spectral indices and LAI for coniferous forests are not applicable to broad-leaf forests.

Figs. 10-13 show the SR values corresponding to the seasonal maximum LAI in August and the seasonal minimum LAI for sites 2, 3-F, 5-F, and 6, respectively, for all four sensors. With the exception of the CASI instrument at site 2, the SR was always higher for the

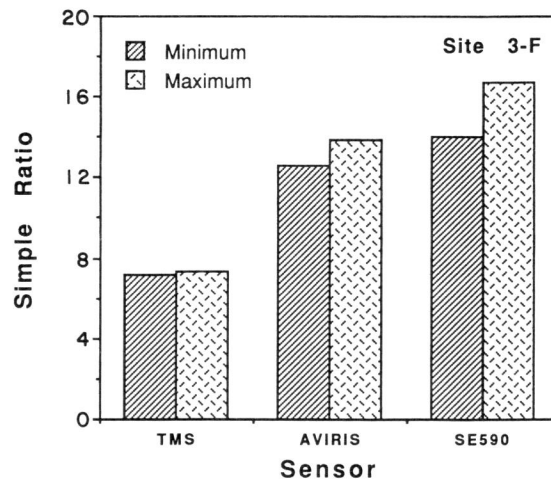


FIG. 11. Seasonal minimum and maximum SR for sensors at site 3-F.

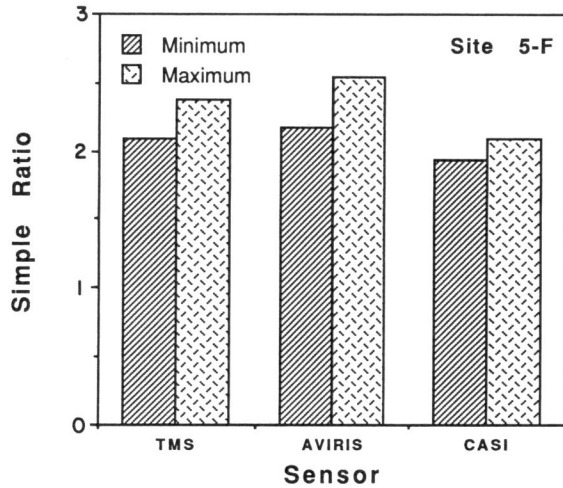


FIG. 12. Seasonal minimum and maximum SR for sensors at site 5-F.

seasonal-maximum time period than it was for the seasonal-minimum time period. It is interesting to note that at site 3-F, with maximum LAI, the TMS sensor readings did not increase much between minimum and maximum LAI, but the AVIRIS and the SE590 did. The LAI increased at site 3-F from 7.4 in the winter to 10.6 in the summer. At both sites 5-F and 6 the instruments responded to the increased LAI between the seasonal minimum and maximum.

CONCLUSION

Strong relationships were observed between the simple ratio (SR) calculated from both broad- and narrow-spectral-band remote-sensing instruments and seasonal leaf area index (LAI) along the Oregon transect. Atmospheric correction of the imagery allowed these diverse sensors to be compared over seasonally and geographically varying atmospheric conditions. The Thematic Mapper Simulator (TMS) SR reached an asymptote at LAI values of 7–8. The Compact Airborne Spectrographic Imager (CASI) and Spectron SE590 radiometer SR continued to increase to the maximum of LAI of 10.6. The Airborne Visible/Infrared Imaging Spectrometer (AVIRIS) SR did not continue to increase with increasing LAI because of the variability of the relationship at LAIs >7. It is difficult to generalize about the form of the relationships between the SR and LAI for the different sensors.

The logarithmic relationships between LAI and the three high-spectral-resolution instruments were similar. The logarithmic relationship between the TMS SR and LAI differed from the high-spectral-resolution instruments because of the lower SR values. The lower SR values were a result of the integration of the TMS over a broad wavelength region and of calibration differences. Scrupulous attention must be paid to instru-

ment calibration standards if we are to generate sensor-independent algorithms or hope to transfer algorithms between sensors. The seasonal trends of the TMS SR deviated from the expected seasonal LAI trends, possibly because of smoke and very low sun elevations. For all of the instruments, however, the SR values from the seasonal maximum and minimum time periods did correspond, almost without exception, to the seasonal LAI.

The strength of the relationships observed between minimum and maximum LAI and the SR calculated from four remote-sensing instruments on three different platforms and at altitudes ranging from 100 m to 20 km indicates that remote sensing offers utility for assessing and monitoring LAI. While we cannot yet develop sensor-independent algorithms, we can use sensor-dependent SR–LAI relationships to extend our results to much larger geographic regions. With proper atmospheric correction, remotely sensed data from a number of narrow- and broad-spectral-band remote-sensing instruments can be used to measure the canopy LAI of coniferous forests.

ACKNOWLEDGMENTS

We wish to express our appreciation for the excellent collaboration of the entire OTTER team. In particular, we are appreciative of the efforts of Greg Olsen, for assistance with the sunphotometer measurements and analysis of the digitized aerial photographs and of the NASA-Ames flight program for their persistence in the acquisition of remotely sensed data during the OTTER MAC. We would also like to express our appreciation for the efforts of Drs. Richard Waring and David Peterson for coordinating the OTTER project, and of Dr. Mel Averner of the Biospherics Research Program and Dr. Diane Wickland of the Biogeochemical Cycling Branch at NASA headquarters for supporting this research. CASI imagery was collected by Borstad Associates, Ltd., and financial support for the ISTS researchers was provided by the

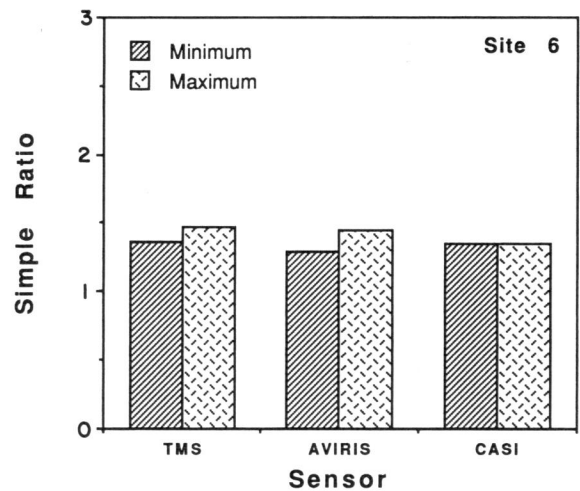


FIG. 13. Seasonal minimum and maximum SR for sensors at site 6.

Ontario Ministry of Industry, Trade and Technology via the Ontario Centres of Excellence Fund and from Itres, Ltd. This research was supported by RTOP number 199-30-72-08 from the NASA Life Sciences Division and from RTOP number 462-43-64-10 from the NASA Earth Science and Applications Division.

## LITERATURE CITED

- Chrien, T., R. Green, and M. Eastwood. 1990. Accuracy of the spectral and radiometric laboratory calibration of the Airborne Visible/Infrared Imaging Spectrometer (AVIRIS). Proceedings Imaging Spectroscopy of the Terrestrial Environment. Pages 37-49 in SPIE [Society of Photo-optical Instrumentation Engineers] publication 1298. International Society for Optical Engineering, Bellingham, Washington, USA.
- Curran, P., and J. Dungan. 1992. Seasonal LAI in slash pine estimated with Landsat TM. *Remote Sensing of Environment* **39**:2-13.
- Diner, D. J., and J. V. Martonchik. 1984. Atmospheric transfer of radiation above an inhomogeneous, non-Lambertian reflective ground: theory. *Journal of Quantitative Spectroscopy and Radiative Transfer* **31**:97-125.
- Fraser, R., and Y. Kaufman. 1985. The relative importance of aerosol scattering and absorption in remote sensing. *IEEE Transactions on Geoscience and Remote Sensing* **GE-23**:625-633.
- Frohlich, C., and G. Shaw. 1980. New determination of Rayleigh scattering in the terrestrial atmosphere. *Applied Optics* **19**:1773-1775.
- Gamon, J. A., C. Field, D. Roberts, S. Ustin, and R. Valentini. 1993. Functional patterns in an annual grassland during an AVIRIS overflight. *Remote Sensing of Environment* **44**:239-253.
- Gholz, H. L. 1982. Environmental limits on aboveground net primary production, leaf area, and biomass in vegetation zones of the Pacific Northwest. *Ecology* **63**:469-481.
- Gholz, H. L., C. C. Grier, A. G. Campbell, and A. T. Brown. 1979. Equations for estimating biomass and leaf area of plants in the Pacific Northwest. Research Paper 41. Forest Research Laboratory, Oregon State University, Corvallis, Oregon, USA.
- Gholz, H. L., S. A. Vogel, W. P. Cropper, K. McKelvey, K. C. Ewel, R. O. Teskey, and P. J. Curran. 1991. Dynamics of canopy structure and light interception of *Pinus elliotti* stands of North Florida. *Ecological Monographs* **61**:33-51.
- Gong, P., R. Pu, and J. Miller. 1992. Correlating leaf area index of Ponderosa pine with hyperspectral CASI data. *Canadian Journal of Remote Sensing* **18**:275-282.
- Green, R., editor. 1990. Retrieval of reflectance from calibrated radiance imagery measured by the Airborne Visible/Infrared Imaging Spectrometer. Pages 107-128 in Proceedings Second AVIRIS Workshop. JPL Publication 90-54. Jet Propulsion Laboratory, Pasadena, California, USA.
- Grier, C. C., and S. W. Running. 1977. Leaf area of mature Northwestern coniferous forests: relation to site water balance. *Ecology* **58**:893-899.
- Herwitz, S. R., D. L. Peterson, and J. R. Eastman. 1989. Thematic Mapper detection of change in the leaf area index of closed canopy pine plantations in central Massachusetts. *Remote Sensing of Environment* **29**:129-140.
- Hoffer, R. M. 1978. Biological and physical considerations in applying computer-aided analysis techniques to remote sensing data. Pages 227-289 in P. Swain and S. Davis, editors. *Remote sensing: the quantitative approach*. McGraw-Hill, New York, New York, USA.
- Johnson, L., C. Hlavka, and D. Peterson. 1994. Multi-variate analysis of AVIRIS data for canopy biochemical estimation along the Oregon transect. *Remote Sensing of Environment*, in press.
- Kneizys, F., E. Shettle, G. Anderson, L. Abrew, J. Chetwynd, J. Shelby, and W. Gallery. 1989. Atmospheric Transmittance/Radiance; Computer Code LOWTRAN 7. Publication number AFGL-TR-88-0177. Environmental Research Papers number 1/1010. Airforce Geophysics Laboratory, Hanscom Air Force Base, Hanscom, Massachusetts, USA.
- Law, B. E., and R. H. Waring. 1994. Remote sensing of leaf area index and radiation intercepted by understory vegetation. *Ecological Applications* **4**:272-279.
- Marshall, J. D., and R. H. Waring. 1986. Comparison of methods of estimating leaf area index in old-growth Douglas-fir. *Ecology* **67**:975-979.
- Matson, P., L. Johnson, C. Billow, J. Miller, and R. Pu. 1994. Seasonal patterns and remote spectral estimation of canopy chemistry across the Oregon transect. *Ecological Applications* **4**:280-298.
- Noxon, J. 1979. Stratospheric NO<sub>2</sub>. 2. Global behavior. *Journal of Geophysical Research* **84**:5067-5076.
- Peterson, D. L., M. A. Spanner, S. W. Running, and K. B. Teuber. 1987. The relationship of Thematic Mapper Simulator data to leaf area index of temperate coniferous forests. *Remote Sensing of Environment* **22**:323-341.
- Peterson, D. L., and R. H. Waring. 1994. Overview of the Oregon Transect Ecosystem Research project. *Ecological Applications* **4**:211-225.
- Ranson, K. C. Daughtry, and L. Biehl. 1986. Sun angle, view angle, and background effects on spectral response of simulated balsam fir canopies. *Photogrammetric Engineering and Remote Sensing* **52**:649-658.
- Running, S. W. 1994. Testing FOREST-BGC ecosystem process simulations across a climatic gradient in Oregon. *Ecological Applications* **4**:238-247.
- Running S. W., D. L. Peterson, M. A. Spanner, and K. B. Teuber. 1986. Remote sensing of forest leaf area index. *Ecology* **67**:273-275.
- Runyon, J., R. H. Waring, S. N. Goward, and J. M. Welles. 1994. Environmental limits on net primary production and light-use efficiency across the Oregon transect. *Ecological Applications* **4**:226-237.
- Russell, P., T. Matsumoto, V. Banta, J. Livingston, C. Mina, D. Colburn, and R. Pueschel. 1986. Measurements with an airborne, autotracking, external-head sunphotometer. Proceedings of the Sixth Conference on Atmospheric Radiation, May, 1986. American Meteorological Society, Boston, Massachusetts, USA.
- Ryan, M. G., and R. H. Waring. 1992. Maintenance respiration and stand development in a subalpine lodgepole pine forest. *Ecology* **73**:2100-2108.
- Spanner, M. A., L. L. Pierce, D. L. Peterson, and S. W. Running. 1990a. Remote sensing of temperate coniferous forest leaf area index: the influence of canopy closure, understory vegetation and background reflectance. *International Journal of Remote Sensing* **11**:95-111.
- Spanner, M. A., L. L. Pierce, S. W. Running, and D. L. Peterson. 1990b. Seasonal trends of AVHRR data of temperate coniferous forests: relationship with leaf area index. *Remote Sensing of Environment* **33**:97-112.
- Sudworth, G. B. 1967. *Forest trees of the Pacific slope*. Dover, Toronto, Ontario, Canada.
- Tanre, D., C. Deroo, P. Duhaut, M. Herman, and J. J. Morcrette. 1990. Description of a computer code to simulate the satellite signal in the solar spectrum: the 5S code. *International Journal of Remote Sensing* **11**:659-668.
- Tucker, C. J. 1979. Red and photographic infrared linear combinations for monitoring vegetation. *Remote Sensing of Environment* **8**:127-150.
- Turner, J., and J. N. Long. 1975. Accumulation of organic matter in a series of Douglas-fir stands. *Canadian Journal of Forest Research* **5**:681-690.

- Vane, G., editor. 1987. Airborne Visible/Infrared Imaging Spectrometer: a description of the sensor, ground data, processing facility, laboratory calibration and first results. JPL Publication 87-38. Jet Propulsion Laboratory, Pasadena, California, USA.
- Van Heuklon, T. 1979. Estimating atmospheric ozone for solar radiation models. *Solar Energy* **22**:63-68.
- Waring, R. H., and J. F. Franklin. 1979. Evergreen coniferous forests of the Pacific Northwest. *Science* **24**:131-140.
- Wrigley, R. C., M. A. Spanner, R. E. Slye, R. Pueschel, and H. R. Aggarwal. 1992. Atmospheric correction of remotely sensed image data by a simplified model. *Journal of Geophysical Research* **97(D17)**:18 797-18 814.

